Journal of Glaciology



Article

Cite this article: Chevrollier L-A, Cook JM, Halbach L, Jakobsen H, Benning LG, Anesio AM, Tranter M (2023). Light absorption and albedo reduction by pigmented microalgae on snow and ice. *Journal of Glaciology* **69**(274), 333–341. https://doi.org/10.1017/jog.2022.64

Received: 30 March 2022
Revised: 5 July 2022
Accepted: 6 July 2022
First published online: 24 August 2022

Keywords:
Glacier modelling; glaciological model experiments; ice biology; melt-surface; snow/ice surface processes

Author for correspondence:
Lou-Anne Chevrollier,
E-mail: lou.chevrollier@envs.au.dk

© The Author(s), 2022. Published by Cambridge University Press. This is an Open Access article, distributed under the terms of the Creative Commons Attribution licence (https://creativecommons.org/licenses/by/4.0/), which permits unrestricted re-use, distribution, and reproduction in any medium, provided the original work is properly cited.

cambridge.org/jog

Light absorption and albedo reduction by pigmented microalgae on snow and ice

Lou-Anne Chevrollier[1], Joseph M. Cook[1], Laura Halbach[1], Hans Jakobsen[2], Liane G. Benning[3,4], Alexandre M. Anesio[1] and Martyn Tranter[1]

[1]Department of Environmental Science, iClimate, Aarhus University, Roskilde, Denmark; [2]Institute for Ecoscience, Aarhus University, Roskilde, Denmark; [3]German Research Centre for Geosciences, GFZ, Potsdam, Germany and [4]Department of Earth Sciences, Free University of Berlin, Berlin, Germany

Abstract

Pigmented microalgae inhabiting snow and ice environments lower the albedo of glacier and ice-sheet surfaces, significantly enhancing surface melt. Our ability to accurately predict their role in glacier and ice-sheet surface mass balance is limited by the current lack of empirical data to constrain their representation in predictive models. Here we present new empirical optical properties for snow and ice algae and incorporate them in a radiative transfer model to investigate their impact on snow and ice surface albedo. We found ice algal cells to be more efficient absorbers than snow algal cells, but their blooms had comparable impact on surface albedo due to the different photic conditions of their habitats. We then used the model to reconstruct the effect of ice algae on bare ice albedo spectra collected at our field site in southern Greenland, where blooms dropped the albedo locally by between 3 and 43%, equivalent to 1–10 L m^{-2} d^{-1} of melted ice. Using the newly parametrized model, future studies could investigate biological albedo reduction and algal quantification from remote hyperspectral and multispectral imagery.

Introduction

Pigmented microalgae thrive on glacier and ice-sheet surfaces worldwide (Hoham and Remias, 2020). They reduce the albedo of snow and ice because their pigments are highly efficient at absorbing solar irradiance (Bidigare and others, 1993; Duval and others, 1999; Remias and others, 2005, 2012b; Yallop and others, 2012; Lutz and others, 2015; Williamson and others, 2020) and they can bloom at high concentrations over large areas (Painter and others, 2001; Takeuchi and others, 2006; Hisakawa and others, 2015; Lutz and others, 2016; Ganey and others, 2017; Huovinen and others, 2018; Wang and others, 2018; Williamson and others, 2018; Cook and others, 2020; Gray and others, 2021). As a result, microalgae blooms can significantly contribute to surface melt, for example producing ~10–13% of run-off in a southwestern site of the Greenland ice sheet (GrIS) (Cook and others, 2020) and ~17% of snow melt at the Harding Icefield in Alaska (Ganey and others, 2017).

Relatively few species are responsible for the albedo reducing effect. Most notable are the dark brown cylindrical algae from the genus *Ancylonema* (Remias and others, 2012a; Yallop and others, 2012; Di Mauro and others, 2020), typically found on ice surfaces and referred to as glacier ice algae, hereafter ice algae; and the green to red spheroidal algae, mostly *Sanguina nivaloides* and *Chloromonas nivalis*, typically inhabiting snow and hereafter referred to as snow algae (Remias and others, 2005; Lutz and others, 2016; Procházková and others, 2019). Both types of algae produce their pigments notably to protect their chloroplasts from damage by high irradiance (Bidigare and others, 1993; Gorton and others, 2001; Gorton and Vogelmann, 2003; Remias and others, 2009, 2012a) and to melt the surrounding ice and snow crystals to locally create a liquid environment promoting growth (Dial and others, 2018; Williamson and others, 2020), thereby potentially fostering positive melt feedbacks as growth enhances surface darkening and causes further melting (Lutz and others, 2014; Ganey and others, 2017).

In general, algal abundance negatively correlates with surface albedo, but cell concentration alone only explains about half of the observed variance in broadband albedo (BBA) (Thomas and Duval, 1995; Lutz and others, 2016; Stibal and others, 2017; Cook and others, 2020). The remainder may be due to the presence of other light-absorbing particulates (LAPs) such as mineral dust and dispersed cryoconite granules (Takeuchi, 2002; Mauro and others, 2017), or changes in the architecture of the snow and ice surface (Tedstone and others, 2020). In order to isolate the different albedo reducing effects, direct measurements of spectral albedo can be reconstructed using a physically based radiative transfer model (RTM) that represents the different mechanisms impacting the surface albedo, so that the role of each mechanism can be determined. Several such RTMs have incorporated biological LAPs onto cryospheric surfaces, for example the Two-streAm Radiative TransfEr in Snow model (TARTES; Libois and others, 2013; Cook and others, 2017b), the physically based snow albedo model (PBSAM; Aoki and others, 2011) or the Snow, Ice and Aerosol Radiative model (SNICAR, Flanner and others, 2007 and BioSNICAR, Cook and others, 2020). Most of these models were developed for snow, but Version 4 of SNICAR introduced the representation of ice as a continuous medium with air bubble inclusions, which accurately reproduces the albedo of glacier ice

(Whicker and others, 2022). However, none of these models have so far included empirically measured optical properties for intact algal cells, limiting our ability to accurately isolate the albedo reduction associated with algal blooms (Cook and others, 2017a).

BioSNICAR calculates biological albedo reduction from cell abundance (cells mL^{-1}) and the optical properties of the cells. These properties are generated from the cell dimensions (μm), cell absorption cross section A_λ (m^2 $cell^{-1}$) and the real part of the cell refractive index n_λ (unitless). A_λ represents the spectral energy absorption for each wavelength λ per cell and determines the biological contribution to the predicted melt. n_λ characterizes scattering at the cell membrane and can typically be assumed wavelength-independent (Hart and Leski, 2006; Dauchet and others, 2015). Both n_λ and A_λ are poorly constrained in the model for snow and ice algae and in particular A_λ, which is currently reconstructed using a pigment mixing model (Cook and others, 2017b; Williamson and others, 2020). This approach does not account for intracellular effects such as the 'pigment packaging' that typically flattens the absorption spectrum of the cells relative to that of their pigments dispersed in solution (Duyens, 1956; Hulst and van de Hulst, 1981; Morel and Bricaud, 1981; Bidigare and others, 1990; Nelson and others, 1993). This effect may decrease ice algae absorption by ~25% (Williamson and others, 2020) and snow algae absorption by up to ~95% (Halbach and others, 2022).

The current lack of *in vivo* optical properties for snow and ice algae cells in numerical models limits our ability to constrain their effect on snow and ice albedo. This work contributes to upgrading the current state-of-the-art in modelling biological albedo reduction by providing the first empirically measured *in vivo* optical properties for snow and ice algae and incorporating them into an existing RTM. The algal optical properties are first used to compare the light-absorption efficiency and packaging effect in snow and ice algae cells. Model simulations are then produced to investigate the relative impact of snow and ice algal blooms on the surface albedo of their respective habitats. Finally, model inversions are performed to evaluate the performance of the model in reproducing algal signature from field measurements and estimate the melt generated locally by algal blooms on bare ice surfaces from the southern ablation area of the GrIS.

Methods

Sample collection and processing

Snow and ice surface samples were collected in the ablation area of the southern part of the GrIS (61.1004 N, −46.8470 E; Fig. S1) between 19th July and 9th August 2021 (details in the Supplementary material). They were transported in the dark in cooling boxes to the home laboratory in Denmark and then preserved in a growth chamber (Percival, USA) at 6°C and with 16:8 h of light:dark cycle (260 μmol s^{-1} m^{-2}) until analyses (1–6 weeks after sample collection). Algal cells were then isolated from the samples by density gradient centrifugation and resuspended in clean water (details in the Supplementary material).

In vivo *absorption cross sections: measurements and calculations*

Transmission spectra T_λ of three independent pigmented algal suspensions (0.62–2.2 $\times 10^5$ cells mL^{-1}) were measured in triplicates in 1 cm pathlength quartz cuvettes (QS101, Hellma Analytics) inserted at the entrance of an integrating sphere mounted in a double beam spectrophotometer (240–850 nm, Shimadzu 2700, 2600-ISR) (details in the Supplementary material). The absorbance (Abs_λ, m^{-1}) was then calculated from the transmission spectra as:

$$\mathrm{Abs}_\lambda = \frac{-1}{l}\ln\left(\frac{T_\lambda}{T_{\lambda,0}}\right) - \mathrm{Abs}_{800}$$

where l is the pathlength of the cuvette, $T_{\lambda,0}$ the transmission spectra of the blank solution (here the cold water used to resuspend the algae) and Abs_{800} the absorbance at 800 nm to correct for the scattering bias (details in the Supplementary material). 16–25 mL of the solution was then filtered at low pressure onto a pre-weighed GF/F filter of diameter 25 mm (Whatman) that was freeze-dried for biomass quantification (kg_{dw} m^{-3}; Mettler Toledo Analytical Balance AE 260). A 1 mL of the solution was used to perform algal cell counts (cells mL^{-1}; 1 mL chamber, Marienfeld Superior) placed under a Nikon Eclipse Ti microscope. The absorbance was then normalized to cell counts and dry weight to obtain respectively a cellular absorption cross section (A_λ, m^2 $cell^{-1}$) and a mass absorption cross section ($A_{\lambda,m}$, m^2 mg_{dw}^{-1}). Cell sizes (μm) and biovolumes (μm^3 $cell^{-1}$) were measured using a FlowCam (Fluid Imaging Technologies Inc.) and ImageJ (Version 1.53) assuming a spherical shape for snow algae and a circular-based cylinder shape for ice algae (Williamson and others, 2018 after Hillebrand and others, 1999; details in the Supplementary material). The algal buoyant density was determined by immersing algae in solutions of Iodixanol (Optiprep, Stem Cell, Proteogenix) of increasing densities until the cells floated. The algal dry densities (kg_{dw} m^{-3}) were calculated by multiplying the algal buoyant densities by the dry fraction x_{dw} (0.59, Gates and others, 1982). The absorption coefficient a_λ (m^{-1}) was finally calculated from A_λ multiplied by the algal dry density and $A_{\lambda,m}$ divided by cell biovolume.

In vitro *absorption cross sections: measurements and calculations*

Pigments were extracted from the GF/F filters used for the biomass quantification described in the previous section, following a procedure adapted from Holzinger and others (2018) and Halbach and others (2022). Briefly, the filters were freeze-dried and preserved at −80° before analysis when they were broken down by repeating bead-beating (60 s) and flash-frozen in liquid nitrogen three times. The lipophilic and hydrophilic phases were extracted with solutions of respectively methyl tertiary-butyl ether with 0.1% of butylated hydroxytoluene and MeOH 20%. The manipulations were performed under a fume hood in the dark in seven steps until the extracts were not visibly coloured anymore (details in the Supplementary material). The transmission spectra of the extracts were analysed as described in the section above and cellular absorption cross sections were then reconstructed by combining the absorbance spectra of both phases corrected for filtration and extraction volumes and normalizing to cell counts. The percent of purpurogallin in ice algal dry weight was calculated from the concentrations in the hydrophilic extracts (mg L^{-1}) using the calibration from Halbach and others (2022) and were then normalized to algal biomass (kg_{dw} m^{-3}).

Calculation and modelling of algal single scattering properties

The distribution of pigments within the cells was assumed homogeneous so that the imaginary part of the refractive index k_λ was directly calculated from the absorption coefficient a_λ (m^{-1}, Bohren and Huffman, 1983):

$$k_\lambda = \frac{\lambda}{4 \times \pi \times a_\lambda}$$

https://doi.org/10.1017/jog.2022.64 Published online by Cambridge University Press

The real part of the refractive index n_λ was estimated by optical densitometry following Hart and Leski (2006) (details in the Supplementary material). The asymmetry parameter g and single scattering albedo w_0 of algae cells were then modelled from the complex refractive index $n_\lambda + ik_\lambda$ of the cells and the cell sizes using the bio-optical model incorporated in the model BioSNICAR. The geometric optics algorithm was chosen for ice algae to represent cells as circular-based cylinder particles (Cook and others, 2020), and Mie theory was chosen for snow algae to represent them as spherical particles (Cook and others, 2017a).

Field spectroscopy and algal abundance measurements

Hemispherical conical reflectance factors (HCRFs) were collected in the study area between 10:00 and 15:20 (solar zenith angle 45–56) using an ASD FieldSpec 4. The spectroradiometer fibre was equipped with a 10° collimating lens held by the arm of a tripod as described in Cook and others (2017a) to avoid self-shading from the instrument. The sensor height was 68–72 cm so that the measurement footprint was $\sim$0.01 m^2. The targeted surfaces were chosen to be roughly homogeneous on a wider surface in order to upscale the results for $\sim$1 m^2 areas, but are not representative of wider surfaces. Incident radiation was measured using a calibrated Spectralon panel and each spectrum was the average of ten measurements. The spectra were post-corrected for the step at 1000 nm (Painter and others, 2001) along with water vapour absorption by polynomial interpolation. For 18 out of 20 spectra, the ice surface was then scraped (1–6 cm) and algal cells were counted as quintuplicates on a full haemocytometer chamber (25 µL per sample – Fuchs-Rosenthal, Lancing, UK), using an upright field microscope (VisiScope100, Model BL124) with a 100× magnification.

Albedo modelling and melt calculations

Albedo modelling was performed using BioSNICAR for two purposes: (a) modelling hypothetical snow and ice surfaces with snow and ice algae blooms to study their relative impact on albedo (parameters in Table S3); and (b) reconstruction of bare ice field HCRF spectra to evaluate the performance of the model in reproducing algal signature and isolate the albedo reducing effect of algal blooms. Because BioSNICAR generates bi-hemispherical albedo, modelled albedo is typically compared to spectral measurements collected using a cosine collector rather than a collimating lens, in order to integrate the back-scattered signal from all directions. This methodology is adapted for snow surfaces but we decided that it was not suitable for the very heterogeneous weathered surface, for the following reasons.

The patches of algae at our specific field site during the fieldwork campaign were rather small, meaning a small footprint was required to ensure the spectrum collected was representative of a homogeneous target surface. However, the signal collected using a cosine collector integrates a signal from a wide surrounding area that differs dramatically from the sampling surface. Reconstructing HCRF spectra with BioSNICAR does mean that we assume either Lambertian scattering or that the narrow nadir view value is representative of the hemispheric value. Evidence in favour of using the HCRF measurements rather than cosine collector albedo measurements are the smaller absolute error between model predictions and our field measurements using the HCRF measurements. We therefore decided that this assumption was more acceptable than assuming surface homogeneity given that we knew the surface to be highly heterogeneous within the cosine collector footprint area. Unfortunately, we cannot provide quantitative estimations of the error from this assumption because we do not know of a reliable way, in the absence of empirical or simulated bidirectional reflectance distribution function (BRDF) or anisotropic reflectance factor data, to gather empirical albedo measurements for our surface types. Since we do not have ice physical and hydrological measurements coupled to the spectra, it was unfortunately not possible to derive a theoretical anisotropy reflectance factor from a model generating BRDF such as DISORT and apply it to our spectra.

We used the adding doubling solver developed by Dang and others (2019) and Whicker and others (2022), allowing to model glacier ice as a continuum with bubble inclusions (layer type = 1 in the model) and snow as a collection of spherical grains (layer type = 0 in the model). In all cases, we parametrized the model with two layers: (1) a 1 mm upper layer of pure ice (density 917 kg m^{-3}) representing a liquid water film where algal cells were added and (2) an ice/snow layer of varying depth, density and bubble/grain size. The irradiance received by the cells from the ice/snow layer was obtained from the upward flux between the layer of ice/snow and the upper millimetre. The illumination used for all simulations was the default SNICAR direct irradiance 'mid-latitude winter' as measurements were collected during cloud-free days. Reconstruction of bare ice HCRF spectra was carried out in two steps, first by inversing the model using a look up table (LUT) to retrieve the 'clean ice' background, and second by running the model in forward mode adding algal abundances measured in the field (when available) at the upper surface, with the sampling depth as a free parameter. For the inversion, the model was run to generate 430 080 spectra that were stored in the LUT (details in the Supplementary material). These spectra were then compared to the field spectra in the near infrared wavelengths (NIR, 800–2500 nm), where algae do not influence the spectral signature. The integrated square error between modelled and measured spectra in the infrared spectral range was then computed, and the chosen modelled albedo corresponded to the one yielding the lowest error while being higher in the visible spectrum. The BBA and instantaneous radiative forcing (IRF, J m^{-2} s^{-1}) were directly obtained as outputs from the model so that the BBA reduction and the IRF due to algae only were calculated by differentiating the outputs of the clean ice scenario to the 'algae loaded' scenario. Daily ice mass loss due to algal cells ΔM (g m^2 d^{-1}) was calculated by integrating the algal IRF from the sunrise ($\sim$04:00) to sunset ($\sim$ 20:00) with a time step of 15 mn, and dividing by the latent heat of fusion of the ice ΔH_{fus} (334 J g^{-1}):

$$\Delta M = \frac{1}{\Delta H_{\text{fus}}} \sum_{sza=88}^{89} IRF(sza) \times \Delta t$$

The IRF was multiplied by Δt = 900 s 15 mn^{-1} to convert it from s^{-1} to 15 mn^{-1} and the 15 min-resolved SZA was retrieved from https://keisan.casio.com/exec/system/1224682277 from the field site coordinates and day of the measurement. Daily mass loss was divided again by the density of water to obtain a volume of meltwater (L m^{-2} d^{-1}) or by the density of ice to obtain a cm-equivalent melt over a m^2 surface (cm w.e. d^{-1}).

Results and discussion

Ice algal cells are more efficient light absorbers than snow algal cells

The absorption cross section A_λ of ice algae cells was higher than that of snow algae cells at all wavelengths, and on average $\sim$2× higher (Fig. 1a). The 'uniquely biological' absorption feature at 670–680 nm, diagnostic of chlorophyll-*a* was apparent in both snow and ice algae absorption spectra, along with the signature of chlorophyll-*b* $\sim$650 nm for snow algae (Painter and others, 2001). The presence of secondary carotenoids in snow algae was

https://doi.org/10.1017/jog.2022.64 Published online by Cambridge University Press

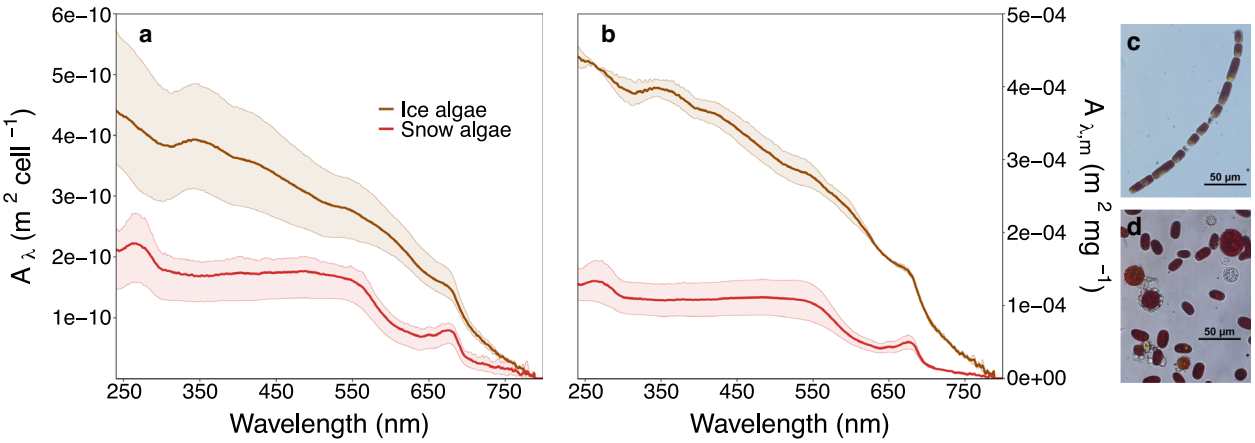


Fig. 1. Ice and snow algae (a) cellular absorption cross section A_λ, and (b) mass absorption cross section $A_{\lambda,m}$. Shaded area corresponds to min. and max. measured coefficients. Microscopy images of (c) ice algae and (d) snow algae from the suspensions analysed.

demonstrated by a broad absorption band in the 300–600 nm spectral range (Gorton and others, 2001; Holzinger and others, 2016) and the presence of phenols in snow and ice algae was evidenced by an increasing absorption towards the UV wavelengths (Duval and others, 1999; Williamson and others, 2020; Halbach and others, 2022). Both algae absorbed broadly across the visible spectral range, maximizing energy harvesting by absorbing strongly where incoming solar energy is greatest. This may have secondary benefits for the algae because most of the energy absorbed is assumed to be conducted to adjacent snow and ice, locally creating a liquid water environment likely promoting growth (Dial and others, 2018; Williamson and others, 2020).

The difference in absorption between the two algae was higher on a per dry mass basis (on average ~3× higher absorption for ice algae; Fig. 1b). This could be due to a higher per cell dry weight of snow algae compared to ice algae (Tables S1 and S2), which is consistent with snow algae typically having a much thicker cell wall and large amounts of lipids associated with their pigments (Remias and others, 2005), evidenced by a lower buoyant density for snow than ice algae (1060 vs 1160 kg m^{-3}). We also found that purpurogallin represented 7.1 ± 0.3% of the total cellular dry weight of ice algae across three suspensions analysed, which is consistent with previous estimates (Williamson and others, 2018) and ~1.75–3.5× higher than for secondary carotenoids in a close relative of snow algae (Hagen and others, 2001; Aflalo and others, 2007). The difference in absorption per dry mass could thus also be due to a lower percent of absorbing pigments in the dry mass of snow algae.

We calculated two estimates of the absorption coefficient a_λ from A_λ and $A_{\lambda,m}$ for each algae (see Methods). These estimates were in excellent agreement (mean error of 2.7 and 9.8% for respectively snow and ice algae; Fig. S2), indicating that the values of A_λ and $A_{\lambda,m}$ are robust. From a_λ, we calculated that snow algae cells would have needed a biovolume on average ~4× higher than ice algae to reach a similar absorption coefficient, assuming a linear relationship between absorption and cell biovolume. This is equivalent to a biovolume of 5748 µm^3 and a cell diameter of ~22 µm for snow algae. However, among the three algal suspensions that were measured to determine triplicates of A_λ (Fig. 1a, Tables S1 and S2), the average cell diameters of snow algae cells were 16.0 ± 2.26, 16.9 ± 3.1 and 21.0 ± 5.9 µm and the highest A_λ was obtained for the solution with the cell diameter of 16.9 ± 3.1 µm. This suggests that A_λ is not linearly positively correlated with cell biovolume and may peak for an intermediate biovolume, which has previously been demonstrated theoretically (Duyens, 1956; Kirk, 1975; Hulst and van de Hulst, 1981) and empirically (Sathyendranath and others, 1987; Bricaud and others, 1988; Stuart and others, 1998; Ciotti and others, 2002), and attributed to the 'packaging effect' (see the next section). In this study, the snow and ice algal cells were of medium size but were collected at the mid to end season and showed a conspicuous dark red (Fig. 1d) and brown (Fig. 1c) pigmentation so that the coefficients A_λ are likely representative of the highly absorbing cells darkening snow and ice surfaces. Thus, our results suggest that an ice algal cell is a more efficient light absorber than a snow algal cell.

Algal pigment absorption is strongly attenuated by a packaging effect, shading intracellular material from high irradiance

Absorption cross sections were reconstructed from pigment extracts for both algae. The typical signatures of secondary carotenoids and phenolics were clearly apparent in the reconstructed coefficients of snow and ice algae respectively (Fig. 2), with an absorption peak ~464 nm for snow algae (Thomas and Duval, 1995) and ~338 nm for ice algae (Halbach and others, 2022). Differences between the measured and reconstructed absorption cross sections represent the difference between *in vivo* and *in vitro* properties, indicating modifications made to the light-absorbing efficiency of the pigment mixture when packaged inside a cell compared to extracted in solution. Here, the reconstructed coefficients were 40 and 5.5 times higher than the *in vivo* coefficients for snow and ice algae respectively at the absorption peaks, suggesting that a strong intracellular pigment packaging effect flattens the spectral signature of both algae (Duyens, 1956), and of snow algae in particular. This effect arises because the pigments are sufficiently concentrated in the cell that the light is significantly attenuated as it travels through the cell, artificially reducing the effective absorption of the algal pigments (Duyens, 1956). For both algae, this strong packaging effect is consistent with previous suggestions that the large amounts of intracellular pigments are used to 'shade' the internal apparatus and protect the cells from damage and overheating (Bidigare and others, 1993; Gorton and others, 2001; Remias and others, 2012a). This effect is especially pronounced when the pigments are abundant (Duyens, 1956; Kirk, 1976; Bricaud and others, 1988), which may explain why snow and ice algal dry densities were significantly higher than green microalgae density (625 ± 12 and 684 ± 12 kg$_{dw}$ m^{-3} for snow and ice algae respectively; 570 kg$_{dw}$ m^{-3} for green microalgae; Hu, 2004). The stronger packaging effect in snow algae was probably due to a larger biovolume and lower surface to volume ratio than ice algae, which reduces the amount of pigments being reached by non-attenuated light (Kirk, 1976). The absorption peaks in the *in vitro* spectra were also spectrally shifted

https://doi.org/10.1017/jog.2022.64 Published online by Cambridge University Press

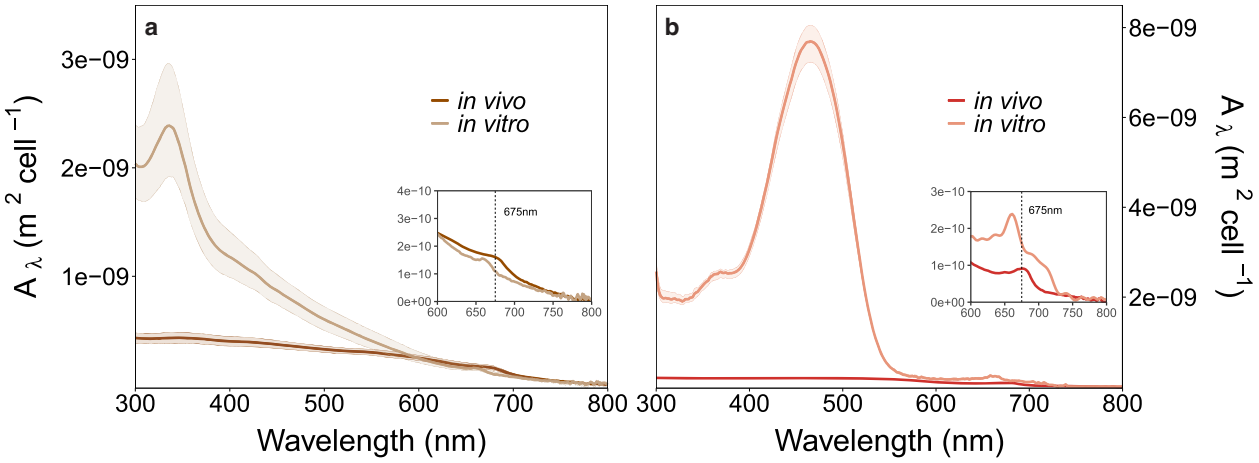


Fig. 2. Differences in *in vivo* and reconstructed A_λ for (a) ice algae and (b) snow algae. Shaded area corresponds to min. and max. measured coefficients.

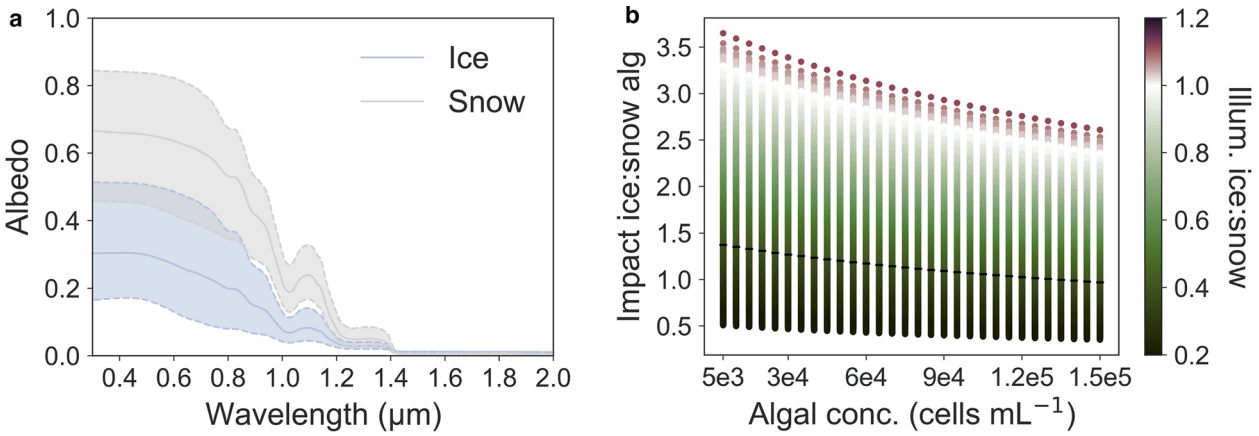


Fig. 3. (a) Ranges of clean snow and ice albedos and (b) ratio of BBA reduction from ice algal blooms to snow algal blooms on their respective habitats as a function of algal concentration and the ratio of illumination received by ice algal cells to that received by snow algal cells. Black ticks in (b) indicate average BBA reduction ratio for each algal concentration.

in comparison with the *in vivo* spectra. The peak of phenolics was shifted by ~12 nm in the ice algal coefficient (from ~350 *in vivo* to ~338 *in vitro*) and the chlorophyll-*a* peak was shifted from ~675 to ~658 nm in both spectra (Fig. 2). The observed spectral shifts are likely the result of a combination between changes made to the pigment assemblages associated with the pigment extraction process (Berner and others, 1989; Bidigare and others, 1990; Ritchie and Sma-Air, 2020) and the effect of the pigment packaging.

These results suggest that reconstructing A_λ from pigment extracts overestimates A_λ and introduces biases in the spectral signature of algae due to spectral shifts. These caveats limit the accuracy of models to predict algal impact on spectral albedo and also prohibit accurate quantification of algae from remote-sensing data because remote quantification relies on the unambiguous detection of pigment signatures.

Ice and snow algae blooms have comparable impact on the surface albedo of their respective habitats

The measurements of a_λ along with the real part of the refractive index n_λ were used to model the single scattering properties of the cells, showing that snow algal cells are more efficient at scattering light (Fig. S3). We then incorporated the optical properties of both algae into a radiative transfer model to compare the albedo lowering efficiency of dark brown ice algal blooms with dark red snow algal blooms. We modelled a wide range of snow and ice albedos (Fig. 3a) and added algal blooms of concentrations between 5×10^3 and 1.5×10^5 cells mL^{-1} (Table S3). The BBA reduction due to ice algal blooms on ice was on average 1.1 ± 0.1 times higher than that of snow algal blooms on snow and that ratio decreased with the concentration (from 1.4 ± 0.5 at 5×10^3 cells mL^{-1} to 0.97 ± 0.32 at 1.5×10^5 cells mL^{-1}; Fig. 3b). The impact of carotenoid-rich snow algal blooms on snow albedo is thus almost equivalent to that of heavily pigmented ice algae blooms on ice albedo, despite snow algae being less efficient absorbers and more efficient scatterers. This is due to the different photic conditions in their respective environments (Fig. 3a). Snowpacks are highly scattering environments where the local irradiance field is naturally enhanced at the surface, which increases the probability of absorption by snow algal cells and enhances the impact of snow algae on albedo (Enríquez and others, 2005; Ehn and Mundy, 2013). This was confirmed by a significant positive relationship between the relative impact of the two algae and the relative irradiance they receive from the ice/snow ($n = 3\,149\,280$, $r^2 = 0.88$, p-value < 0.001; Fig. 3b). In general, snow algal cells receive more light because of their environment (ratio < 1 in Fig. 3b) but when the light available to the cells is equal (ratio of 1 in Fig. 3b), ice algae absorb ~2.7 times more than snow algae at equivalent abundance, because they are more efficient absorbers (Fig. 1).

Ice algae blooms locally dropped bare ice albedo by 3.5–43% at our field site, generating 1.2–9.7 L m^{-2} d^{-1}

We used the model to reconstruct our bare ice field spectra and prescribed cell concentrations from samples taken at each surface

https://doi.org/10.1017/jog.2022.64 Published online by Cambridge University Press

when available (18 spectra out of 20; Table S4). The model recreated these spectra very accurately (Fig. 4; mean standard error = 0.007 ($n = 20$), Table S4), and in particular the algal spectral features, including the specific chlorophyll-*a* peak. The remaining error in the visible spectrum could be related to the uncertainties on the retrieved ice surface properties, or the presence of other LAPs such as mineral dust. Since this error was small, our simulations support previous findings that the dust associated with algal blooms on the GrIS does not significantly lower the albedo above 350 nm (Yallop and others, 2012; Stibal and others, 2017; Cook and others, 2020). We also reproduced similar spectra gathered in the dark zone of the GrIS (38 km inland of the margin near Kangerlussuaq in July 2017; Cook and others, 2020) and similar agreement between measured and modelled spectra was observed (Fig. S4).

The biological signature in the tested field spectra was exclusively that of ice algae because snow algae concentrations were always low at the sampling sites (< 1400 cells mL^{-1}) with a subsequent negligible impact on the BBA. We found that ice algae reduced the surface albedo between 3.5 and 43% at our field site from surfaces where measured concentrations ranged 3×10^3–1×10^5 cells mL^{-1}, representative of concentrations typically measured on bare ice on the GrIS, although higher concentrations have been measured in the dark zone (Yallop and others, 2012; Stibal and others, 2017; Williamson and others, 2020). The range of BBA reduction was 0.012–0.099 (Table S4). These results quantify the direct albedo lowering effect of ice algae, which takes into account only the additional absorption of light caused by the presence of the algae. This method allows biological albedo reduction to be isolated from the ice physical configuration, which can

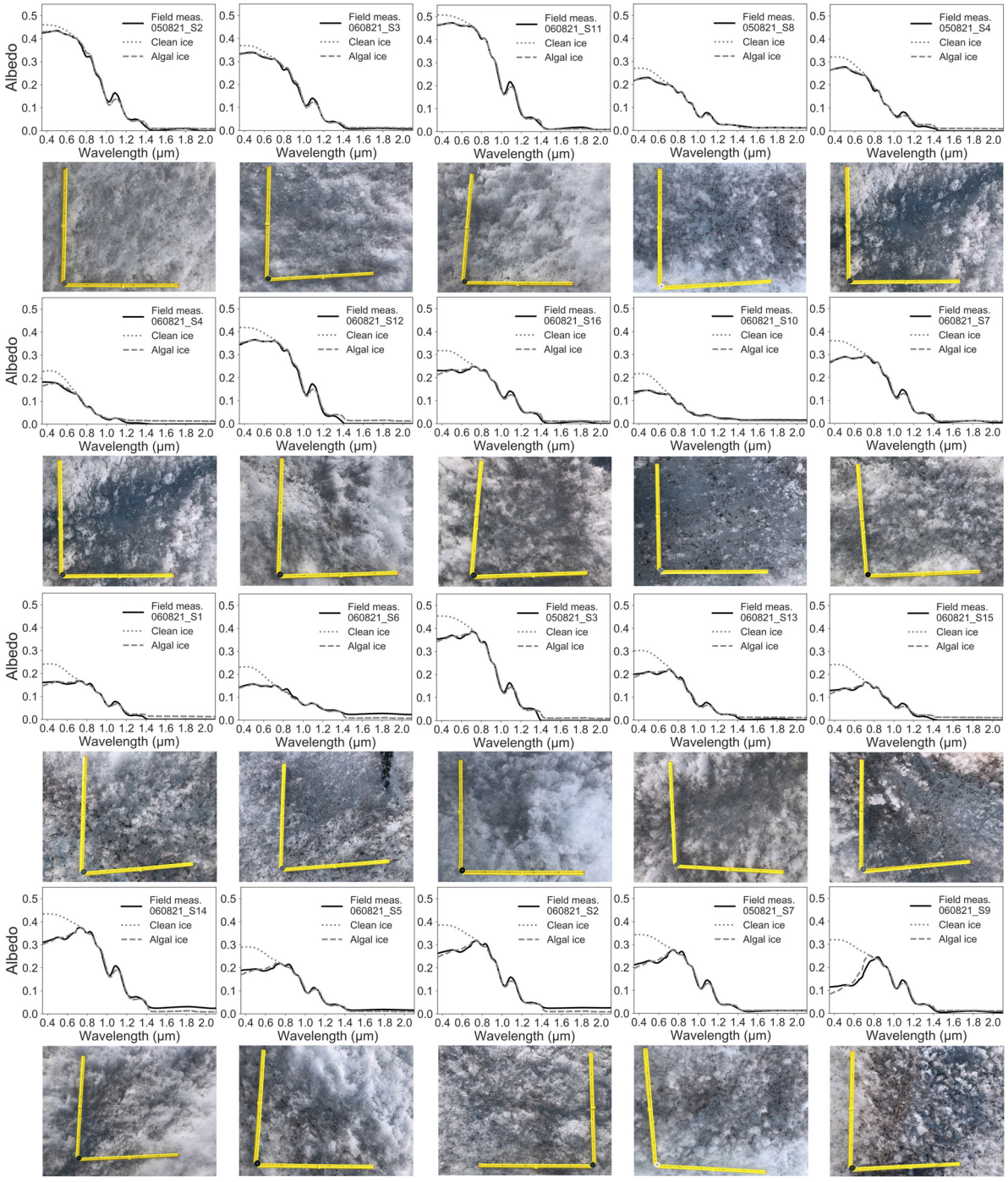


Fig. 4. Field vs modelled spectra for bare ice surfaces from our field site. Length of scale: 50 cm.

https://doi.org/10.1017/jog.2022.64 Published online by Cambridge University Press

change dramatically as the surface 'weathering crust' develops and decays, significantly driving the BBA of bare ice surfaces (Tedstone and others, 2020). Indeed, the BBA of the reconstructed 'clean ice' varied by 65%, while the BBA of 'algal ice' (i.e. clean ice to which algal concentrations were added in the model) varied by 73% among the 20 spectra. Thus, most of the variability was attributed to the ice structure. This likely explains why we found that field-measured algal counts were not a good predictor of the BBA ($r^2 = 0.20$, p-value $= 0.06$, $n = 18$, Fig. S5a). The correlation improved when correcting the algal abundance for the sampling depth (Table S4), but remained poor overall ($r^2 = 0.43$, p-value $= 0.003$, $n = 18$, Fig. S5b). As a result, a given concentration of ice algal cells can be associated with a wide range of BBAs depending on the ice surface type and the time of the measurement, which is why the algal signature needs to be isolated to estimate algal radiative forcing.

We integrated the algal radiative forcing over an entire day yielding melt equivalents of 1.2–9.7 L m^{-2} d^{-1}. Some 15% of the daily melt produced by the addition of algae was not explained by algal abundance in our model inversions (Fig. S5c). In addition, the ratio of BBA reduction to algal concentration, which represents the algal efficiency in reducing albedo, was almost fully predicted by the illumination received from the ice ($r^2 = 0.93$, p-value < 0.0001, $n = 18$, Fig. S5d). This 15% can thus be attributed to the effect of the ice surface that indirectly impacts the biological albedo reduction by changing the photic conditions, as discussed in the previous section. The equivalent surface lowering over a day was 0.13–1.1 cm w.e. d^{-1} assuming that the surface is pure ice with a density of 917 kg m^{-3}. The density of the weathering crust is however typically lower than pure ice (Cooper and others, 2018), and ice algae were responsible for equivalent surface lowering of 0.17–1.7 cm w.e. d^{-1} after correcting the surface lowering to the density retrieved by the model for each surface (Table S4). These values are in excellent agreement with previous estimates from the dark zone of 0.03–1.9 cm w.e. d^{-1} (Cook and others, 2020; Williamson and others, 2020).

New opportunities

BioSNICAR is now able to reproduce ice algal signature from hyperspectral measurements on bare ice surfaces. This opens up new possibilities to investigate the role of algae on ice melt and in particular, model inversions may enable estimations of the biological albedo reduction from hyperspectral remote-sensing imagery. In addition, the model can now be used to develop algorithms able to predict algal abundance from satellite multispectral imagery, enabling population dynamics to be examined at the regional scale and beyond. However, the error associated with the direct comparison of directional reflectance measurements to hemispherical albedo modelled by BioSNICAR needs to be better constrained, by measuring reflectance from different angles to estimate the BRDF or by deriving the latter from a radiative transfer model with angular definition. We also show that the ice parameters retrieved by BioSNICAR, in particular the density, are consistent with previously published data (Table S4; Cooper and others, 2018). However, empirical measurements of the ice physical properties for each of our sample sites were not available for direct validation of our retrievals. This is a priority research goal that, once completed, will enable our model to be used to investigate the relationships between algal abundance and the physics of the weathered crust and better understand the melting feedbacks between them. Daily surface melt calculations are based on the assumption of constant algal concentration and distribution as well as ice physical configuration throughout the day but they suggest that low algal concentrations can melt more than 1 kg of ice per m^2 per day, which is likely to significantly change the ice physical structure and potentially redistribute algal cells on the surface. These feedbacks are not accounted for in our study and their implementation is an important avenue for future refinements of our model. Finally, coupling BioSNICAR to algal growth, surface mass balance and meteorological models might enable algal albedo reducing effects to be predicted into the future.

Conclusion

We presented the first empirical *in vivo* optical properties of the two major biological albedo reducers on snow and ice using an integrative approach, accounting for natural variability associated with cell orientation, size, pigment content and packaging effects. Both algae broadly absorbed in the spectral range where solar irradiance peak, suggesting that their pigments allow them to maximize absorption and heat conduction in order create a local liquid environment promoting growth. These pigments also have a photoprotective role as they absorb most of the light passing through the cell, shading the algal internal apparatus behind from damage and overheating. This shading or packaging effect was demonstrated by a strong flattening of the *in vivo* spectra in comparison with the *in vitro* spectra, in particular for snow algae. We found that snow algae cells are less efficient absorbers than ice algal cells, yet their blooms had comparable impact on the surface albedo due to the differences in photic conditions of their respective habitats. The reconstruction of bare ice field spectra using the new algal optical properties demonstrated the high efficiency of ice algae in absorbing light and melting ice. At our field site in the ablation zone of the southern GrIS, ice algae populations locally dropped the BBA by between 3.5 and 43%, corresponding to a melt generation of 1.2–9.7 L m^{-2} d^{-1}. The reconstruction method presented using BioSNICAR allows to isolate and accurately quantify the impact of algal blooms on biological albedo reduction but the error associated with the direct comparison of bi-hemispherical albedo to directional reflectance needs to be better constrained. The method could then be used on remote-sensed hyperspectral data to upscale the estimates presented in this study, in particular in the dark zone of the GrIS where ice algae are blooming on wide areas of the ice surface.

Supplementary material. The supplementary material for this article can be found at https://doi.org/10.1017/jog.2022.64

Data availability. The version 2.0 of the model BioSNICAR used in this work including microalgae optical properties is freely available at https://doi.org/10.5281/zenodo.6390293. Field spectra are available on request at lou.chevrollier@envs.au.dk.

Acknowledgements. This work is part of the project DeepPurple that has received funding from the European Research Council (ERC) under the European Union's Horizon 2020 research and innovation programme (Grant agreement No. 856416). LC thanks Marie B. Jensen and Laura Perini for the valuable support with field data collection and laboratory manipulations, Pr. Stiig Markager for lending the laboratory instruments and providing useful advices for the bio-optical experiments, as well as L. Schlyter and S. Feng for the map generation.

Author contributions. LC and JC designed the study. LC performed field, modelling and laboratory experiments, analysed the data, produced the figures and wrote the first draft. JC wrote code, produced the model documentation and guided the manuscript preparation and field data collection. LH contributed to data interpretation and guided the pigment extraction. HJ guided the FlowCam and the microscope use and provided useful advice on the experimental design. MT provided helpful guidance on the fieldwork design and refined the manuscript. AA and LB helped with data collection in the field. All authors contributed to the final manuscript.

References

Aflalo C, Meshulam Y, Zarka A and Boussiba S (2007) On the relative efficiency of two- vs. one-stage production of astaxanthin by the green alga *Haematococcus pluvialis*. *Biotechnology and Bioengineering* **98**(1), 300–305. doi: 10.1002/bit.21391

Aoki T, and 5 others (2011) Physically based snow albedo model for calculating broadband albedos and the solar heating profile in snowpack for general circulation models. *Journal of Geophysical Research: Atmospheres* **116**(D11), 015507. doi: 10.1029/2010JD015507

Berner T, Dubinsky Z, Wyman K and Falkowski PG (1989) Photoadaptation and the 'package' effect in *Dunaliella tertiolecta* (Chlorophyceae). *Journal of Phycology* **25**(1), 70–78. doi: 10.1111/j.0022-3646.1989.00070.x

Bidigare RR, Ondrusek ME, Morrow JH and Kiefer DA (1990) In-vivo absorption properties of algal pigments. *Ocean Optics X* **1302**, 290–302. doi: 10.1117/12.21451

Bidigare RR, and 6 others (1993) Evidence a photoprotective for secondary carotenoids of snow algae. *Journal of Phycology* **29**(4), 427–434. doi: 10.1111/j.1529-8817.1993.tb00143.x

Bohren CF and Huffman DR (1983) *Absorption and scattering of light by small particles*. John Wiley and Sons, Inc.

Bricaud A, Bédhomme AL and Morel A (1988) Optical properties of diverse phytoplanktonic species: experimental results and theoretical interpretation. *Journal of Plankton Research* **10**(5), 851–873. doi: 10.1093/plankt/10.5.851

Ciotti AM, Lewis MR and Cullen JJ (2002) Assessment of the relationships between dominant cell size in natural phytoplankton communities and the spectral shape of the absorption coefficient. *Limnology and Oceanography* **47**(2), 404–417. doi: 10.4319/lo.2002.47.2.0404

Cook JM, and 9 others (2017a) Quantifying bioalbedo: a new physically based model and discussion of empirical methods for characterising biological influence on ice and snow albedo. *The Cryosphere* **11**(6), 2611–2632. doi: 10.5194/tc-11-2611-2017

Cook JM, Hodson AJ, Taggart AJ, Mernild SH and Tranter M (2017b) A predictive model for the spectral 'bioalbedo' of snow. *Journal of Geophysical Research: Earth Surface* **122**(1), 434–454. doi: 10.1002/2016JF003932

Cook JM, and 23 others (2020) Glacier algae accelerate melt rates on the south western Greenland ice sheet. *The Cryosphere* **14**(1), 309–330. doi: 10.5194/tc-14-309-2020

Cooper MG, and 7 others (2018) Meltwater storage in low-density near-surface bare ice in the Greenland ice sheet ablation zone. *The Cryosphere* **12**(3), 955–970. doi: 10.5194/tc-12-955-2018

Dang C, Zender CS and Flanner MG (2019) Intercomparison and improvement of two-stream shortwave radiative transfer schemes in earth system models for a unified treatment of cryospheric surfaces. *The Cryosphere* **13**, 2325–2343. doi: 10.5194/tc-13-2325-2019

Dauchet J, Blanco S, Cornet JF and Fournier R (2015) Calculation of the radiative properties of photosynthetic microorganisms. *Journal of Quantitative Spectroscopy and Radiative Transfer* **161**, 60–84. doi: 10.1016/j.jqsrt.2015.03.025

Dial RJ, Ganey GQ and Skiles SM (2018) What color should glacier algae be? An ecological role for red carbon in the cryosphere. *FEMS Microbiology Ecology* **94**(3), fiy007. doi: 10.1093/femsec/fiy007

Di Mauro B, and 8 others (2020) Glacier algae foster ice-albedo feedback in the European Alps. *Scientific Reports* **10**, 4739. doi: 10.1038/s41598-020-61762-0

Duval B, Shetty K and Thomas WH (1999) Phenolic compounds and antioxidant properties in the snow alga *Chlamydomonas nivalis* after exposure to UV light. *Journal of Applied Phycology* **11**(6), 559–566. doi: 10.1023/A:1008178208949

Duyens LNM (1956) The flattering of the absorption spectrum of suspensions, as compared to that of solutions. *Biochimica et Biophysica Acta* **19**, 1–12. doi: 10.1016/0006-3002(56)90380-8

Ehn JK and Mundy CJ (2013) Assessment of light absorption within highly scattering bottom sea ice from under-ice light measurements: implications for Arctic ice algae primary production. *Limnology and Oceanography* **58**(3), 893–902. doi: 10.4319/lo.2013.58.3.0893

Enríquez S, Méndez ER and Iglesias-Prieto RI (2005) Multiple scattering on coral skeletons enhances light absorption by symbiotic algae. *Limnology and Oceanography* **50**(4), 1025–1032. doi: 10.4319/lo.2005.50.4.1025

Flanner MG, Zender CS, Randerson JT and Rasch PJ (2007) Present-day climate forcing and response from black carbon in snow. *Journal of Geophysical Research: Atmospheres* **112**(D11), 08003. doi: 10.1029/2006JD008003

Ganey GQ, Loso MG, Burgess AB and Dial RJ (2017) The role of microbes in snowmelt and radiative forcing on an Alaskan icefield. *Nature Geoscience* **10**, 754–759. doi: 10.1038/ngeo3027

Gates MA, Rogerson A and Berger J (1982) Dry to wet weight biomass conversion constant for *Tetrahymena elliotti* (Ciliophora, Protozoa). *Oecologia* **55**(2), 145–148. doi: 10.1007/BF00384479

Gorton HL and Vogelmann TC (2003) Ultraviolet radiation and the snow alga *Chlamydomonas nivalis* (Bauer) Wille. *Photochemistry and Photobiology* **77**(6), 608–615. doi: 10.1562/0031-8655(2003)0770608URATSA2.0.CO2

Gorton HL, Williams WE and Vogelmann TC (2001) The light environment and cellular optics of the snow alga *Chlamydomonas nivalis* (Bauer) Wille. *Photochemistry and Photobiology* **73**(6), 611–620. doi: 10.1562/0031-8655(2001)0730611TLEACO2.0.CO2

Gray A, and 7 others (2021) Remote sensing phenology of Antarctic green and red snow algae using worldview satellites. *Frontiers in Plant Science* **12**, 877. doi: 10.3389/fpls.2021.671981

Hagen C, Grünewald K, Xyländer M and Rothe E (2001) Effect of cultivation parameters on growth and pigment biosynthesis in flagellated cells of *Haematococcus pluvialis*. *Journal of Applied Phycology* **13**(1), 79–87. doi: 10.1023/A:1008105909044

Halbach L, and 14 others (2022) Pigment signatures of algal communities and their implications for glacier surface darkening, in review. *Scientific Reports*.

Hart SJ and Leski TA (2006) Refractive index determination of biological particles. Technical report, Naval Research Lab, Washington, DC.

Hillebrand H, Dürselen CD, Kirschtel D, Pollingher U and Zohary T (1999) Biovolume calculation for pelagic and benthic microalgae. *Journal of Phycology* **35**(2), 403–424. doi: 10.1046/j.1529-8817.1999.3520403.x

Hisakawa N, and 7 others (2015) Metagenomic and satellite analyses of red snow in the Russian Arctic. *PeerJ* **3**, e1491. doi: 10.7717/peerj.1491

Hoham RW and Remias D (2020) Snow and glacial algae: a review. *Journal of Phycology* **56**(2), 264–282. doi: 10.1111/jpy.12952

Holzinger A, Allen MC and Deheyn DD (2016) Hyperspectral imaging of snow algae and green algae from aeroterrestrial habitats. *Journal of Photochemistry and Photobiology B: Biology* **162**, 412–420. doi: 10.1016/j.jphotobiol.2016.07.001

Holzinger A, and 6 others (2018) Arctic, Antarctic, and temperate green algae *Zygnema* spp. under UV-B stress: vegetative cells perform better than pre-akinetes. *Protoplasma* **255**(4), 1239–1252. doi: 10.1007/s00709-018-1225-1

Hu W (2004) *Dry weight and cell density of individual algal and cyanobacterial cells for algae research and development*. Master's thesis, University of Missouri-Columbia, https://hdl.handle.net/10355/46477.

Huovinen P, Ramírez J and Gómez I (2018) Remote sensing of albedo-reducing snow algae and impurities in the maritime Antarctica. *ISPRS Journal of Photogrammetry and Remote Sensing* **146**, 507–517. doi: 10.1016/j.isprsjprs.2018.10.015

Kirk JTO (1975) A theoretical analysis of the contribution of algal cells to the attenuation of light within natural waters: I. General treatment of suspensions of pigmented cells. *New Phytologist* **75**(1), 11–20. doi: 10.1111/j.1469-8137.1975.tb01366.x

Kirk JTO (1976) A theoretical analysis of the contribution of algal cells to the attenuation of light within natural waters: III. Cylindrical and spheroidal cells. *New Phytologist* **77**(2), 341–358. doi: 10.1111/j.1469-8137.1976.tb01524.x

Libois Q, and 6 others (2013) Influence of grain shape on light penetration in snow. *The Cryosphere* **7**(6), 1803–1818. doi: 10.5194/tc-7-1803-2013

Lutz S, Anesio AM, Field K and Benning LG (2015) Integrated 'omics', targeted metabolite and single-cell analyses of Arctic snow algae functionality and adaptability. *Frontiers in Microbiology* **6**, 1323. doi: 10.3389/fmicb.2015.01323

Lutz S, Anesio AM, Villar SEJ and Benning LG (2014) Variations of algal communities cause darkening of a Greenland glacier. *FEMS Microbiology Ecology* **89**(2), 402–414. doi: 10.1111/1574-6941.12351

Lutz S, and 6 others (2016) The biogeography of red snow microbiomes and their role in melting Arctic glaciers. *Nature Communications* **7**, 11968. doi: 10.1038/ncomms11968

Mauro BD, and 7 others (2017) Impact of impurities and cryoconite on the optical properties of the Morteratsch Glacier (Swiss Alps). *The Cryosphere* **11**(6), 2393–2409. doi: 10.5194/tc-11-2393-2017

Morel A and Bricaud A (1981) Theoretical results concerning light absorption in a discrete medium, and application to specific absorption of phytoplankton. *Deep Sea Research Part A: Oceanographic Research Papers* **28**(11), 1375–1393. doi: 10.1016/0198-0149(81)90039-X

https://doi.org/10.1017/jog.2022.64 Published online by Cambridge University Press

Nelson NB, Prézelin BB and Bidigare RR (1993) Phytoplankton light absorption and the package effect in California coastal waters. *Marine Ecology Progress Series* **38**, 217–227. doi: 10.4054/DemRes.2018.38.53

Painter TH, and 5 others (2001) Detection and quantification of snow algae with an airborne imaging spectrometer. *Applied and Environmental Microbiology* **67**(11), 5267–5272. doi: 10.1128/AEM.67.11.5267-5272.2001

Procházková L, Leya T, Křížková H and Nedbalová L (2019) *Sanguina nivaloides* and *Sanguina aurantia* Gen. et spp. nov. (Chlorophyta): the taxonomy, phylogeny, biogeography and ecology of two newly recognised algae causing red and orange snow. *FEMS Microbiology Ecology* **95**(6), fiz064. doi: 10.1093/femsec/fiz064

Remias D, Lütz-Meindl U and Lütz C (2005) Photosynthesis, pigments and ultrastructure of the alpine snow alga *Chlamydomonas nivalis*. *European Journal of Phycology* **40**(3), 259–268. doi: 10.1080/09670260500202148

Remias D, Holzinger A and Lütz C (2009) Physiology, ultrastructure and habitat of the ice alga *Mesotaenium berggrenii* (Zygnemaphyceae, Chlorophyta) from glaciers in the European Alps. *Phycologia* **48**(4), 302–312. doi: 10.2216/08-13.1

Remias D, Holzinger A, Aigner S and Lütz C (2012a) Ecophysiology and ultrastructure of *Ancylonema nordenskiöldii* (Zygnematales, Streptophyta), causing brown ice on glaciers in Svalbard (High Arctic). *Polar Biology* **35** (6), 899–908. doi: 10.1007/s00300-011-1135-6

Remias D, and 5 others (2012b) Characterization of an UV-and VIS-absorbing, purpurogallin-derived secondary pigment new to algae and highly abundant in *Mesotaenium berggrenii* (Zygnematophyceae, Chlorophyta), an extremophyte living on glaciers. *FEMS Microbiology Ecology* **79**(3), 638–648. doi: 10.1111/j.1574-6941.2011.01245.x

Ritchie RJ and Sma-Air S (2020) Using integrating sphere spectrophotometry in unicellular algal research. *Journal of Applied Phycology* **32**(5), 2947–2958. doi: 10.1007/s10811-020-02232-y

Sathyendranath S, Lazzara L and Prieur L (1987) Variations in the spectral values of specific absorption of phytoplankton. *Limnology Oceanography* **32**, 403–415. doi: 10.4319/lo.1987.32.2.0403

Stibal M, and 17 others (2017) Algae drive enhanced darkening of bare ice on the Greenland ice sheet. *Geophysical Research Letters* **44**(22), 11–463. doi: 10.1002/2017GL075958

Stuart V, Sathyendranath S, Platt T and Irwin BD (1998) Pigments and species composition of natural phytoplankton populations: effect on the absorption spectra. *Journal of Plankton Research* **20**(2), 187–217. doi: 10.1093/plankt/20.2.187

Takeuchi N (2002) Optical characteristics of cryoconite (surface dust) on glaciers: the relationship between light absorbency and the property of organic matter contained in the cryoconite. *Annals of Glaciology* **34**, 409–414. doi: 10.3189/172756402781817743

Takeuchi N, Dial RJ, Kohshima S and Uetake J (2006) Spatial distribution and abundance of red snow algae on the Harding icefield, Alaska derived from a satellite image. *Geophysical Research Letters* **33**(21), 754–759. doi: 10.1029/2006GL027819

Tedstone AJ, and 7 others (2020) Algal growth and weathering crust state drive variability in western Greenland ice sheet ice albedo. *The Cryosphere* **14**(2), 521–538. doi: 10.5194/tc-14-521-2020

Thomas WH and Duval B (1995) Sierra Nevada, California, USA, snow algae: snow albedo changes, algal–bacterial interrelationships, and ultraviolet radiation effects. *Arctic and Alpine Research* **27**(4), 389–399.

van de Hulst HC (1981) *Light scattering by small particles*. New York: Dover Publications, Inc.

Wang S, Tedesco M, Xu M and Alexander PM (2018) Mapping ice algal blooms in southwest Greenland from space. *FEMS Microbiology Ecology* **45**(21), 11–779. doi: 10.1029/2018GL080455

Whicker CA, and 5 others (2022) SNICAR-ADv4: a physically based radiative transfer model to represent the spectral albedo of glacier ice. *The Cryosphere* **16**, 1197–1220. doi: 10.5194/tc-16-1197-2022

Williamson CJ, and 8 others (2018) Ice algal bloom development on the surface of the Greenland ice sheet. *FEMS Microbiology Ecology* **94**(3), fiy025. doi: 10.1093/femsec/fiy025

Williamson CJ, Cook JM, Tedstone AJ and Anesio A (2020) Algal photophysiology drives darkening and melt of the Greenland ice sheet. *Proceedings of the National Academy of Sciences* **117**(11), 5694–5705. doi: 10.1073/pnas.1918412117

Yallop M, and 13 others (2012) Photophysiology and albedo-changing potential of the ice algal community on the surface of the Greenland ice sheet. *The ISME Journal* **6**, 2302–2313. doi: 10.1038/ismej.2012.107

https://doi.org/10.1017/jog.2022.64 Published online by Cambridge University Press